Transgenic Quail as a Model for Research in the Avian Nervous System: A Comparative Study of the Auditory Brainstem

Armin H. Seidl,[1,2] Jason Tait Sanchez,[1,2] Leslayann Schecterson,[1,3] Kathryn M. Tabor,[1,2] Yuan Wang,[1,2] Daniel T. Kashima,[1,2] Greg Poynter,[5] David Huss,[5] Scott E. Fraser,[5] Rusty Lansford,[5] and Edwin W. Rubel[1,2,4]*

[1]Virginia Merrill Bloedel Hearing Research Center, University of Washington, Seattle, Washington 98195
[2]Otolaryngology-Head & Neck Surgery, University of Washington, Seattle, Washington 98195
[3]Institute for Stem Cell and Regenerative Medicine, University of Washington, Seattle, Washington 98195
[4]Department of Physiology and Biophysics, University of Washington, Seattle, Washington 98195
[5]Biological Imaging Center, Division of Biology, California Institute of Technology, Pasadena, California 91125

ABSTRACT

Research performed on transgenic animals has led to numerous advances in biological research. However, using traditional retroviral methods to generate transgenic avian research models has proved problematic. As a result, experiments aimed at genetic manipulations on birds have remained difficult for this popular research tool. Recently, lentiviral methods have allowed the production of transgenic birds, including a transgenic Japanese quail (*Coturnix coturnix japonica*) line showing neuronal specificity and stable expression of enhanced green fluorescent protein (eGFP) across generations (termed here *GFP quail*). To test whether the GFP quail may serve as a viable alternative to the popular chicken model system, with the additional benefit of genetic manipulation, we compared the development, organization, structure, and function of a specific neuronal circuit in chicken (*Gallus gallus domesticus*) with that of the GFP quail. This study focuses on a well-defined avian brain region, the principal nuclei of the sound localization circuit in the auditory brainstem, nucleus magnocellularis (NM), and nucleus laminaris (NL). Our results demonstrate that structural and functional properties of NM and NL neurons in the GFP quail, as well as their dynamic properties in response to changes in the environment, are nearly identical to those in chickens. These similarities demonstrate that the GFP quail, as well as other transgenic quail lines, can serve as an attractive avian model system, with the advantage of being able to build on the wealth of information already available from the chicken. J. Comp. Neurol. 521:5–23, 2013.

INDEXING TERMS: transgenic quail; auditory brainstem

Transgenic model systems, such as mice, fish, worms, and flies, have had a remarkable impact on the study of biology in recent decades (Jaenisch, 1988; Dunn et al., 2005). Mice that express green fluorescent protein (GFP) in neurons have helped tremendously to address questions about neuronal structure and function in both adult (e.g., Feng et al., 2000; Grutzendler et al., 2002; Trachtenberg et al., 2002) and developing brains (e.g., Lendvai et al., 2000; Portera-Cailliau et al., 2005; Nägerl et al., 2007).

Despite their impact, traditional transgenic methods have proved problematic for many popular research species, such as birds, methods for which have remained almost entirely elusive (Sang, 2004). During the last three

The first five authors contributed equally to this work.

Dr. Sanchez's current address is Knowles Hearing Center, Department of Communication Sciences and Disorders, Northwestern University, Frances Searle Building, 2240 Campus Drive. Evanston, IL 60208.

D.T. Kashima's current address is Vanderbilt School of Medicine, 215 Light Hall, Nashville, TN 37232.

Grant sponsor: National Institute on Deafness and Other Communication Disorders, U.S. Public Health Service; Grant numbers: R01 DC03829 and Research Core Center DC04661; Grant sponsor: National Center for Research Resources, National Institutes of Health; Grant number: R21HD047347-01; Grant sponsor: Center of Excellence in Genomic Science, National Institutes of Health; Grant number: P50 HG004071; Grant sponsor: National Institute of Dental and Craniofacial Research; Grant number: FaceBase U01 DE020063.

*CORRESPONDENCE TO: Edwin W. Rubel, Virginia Merrill Bloedel Hearing Research Center, University of Washington, Box 357923, Seattle, WA 98195-7923. E-mail: rubel@uw.edu

Received April 25, 2012; Revised June 26, 2012; Accepted July 6, 2012
DOI 10.1002/cne.23187
Published online July 14, 2012 in Wiley Online Library (wileyonlinelibrary.com)

decades, production of transgenic chicken was attempted by using a number of retroviral vectors. However, transfection efficiency was generally low (Salter et al., 1987; Bosselman et al., 1989; Perry and Sang, 1993; Zajchowski and Etches, 2000; Mozdziak et al., 2003). More recently, a simple and effective method for producing transgenic birds by using lentiviral vectors has been introduced (Scott and Lois, 2005; Poynter et al., 2009). The transgenic Japanese quail (Coturnix coturnix japonica) expresses enhanced GFP (eGFP) driven by the human synapsin I gene promoter. The consistent expression of eGFP is specific to neurons throughout development and into maturation and is sufficient to visualize individual axons and dendrites. Thus, fluorescently labeled neurons will allow for more in-depth studies of neuron migration, axonal pathways, dendritic structure, and synaptogenesis in both fixed and living tissue.

In order to evaluate and promote the use of transgenic quail as a useful avian model to study brain development, structure, and function, we examined how specific neurons in the GFP quail compared with equivalent neurons in a member of the same taxonomic family, the white leghorn chicken (Phasianidae, Gallus gallus domesticus), a widely used species in biological research, particularly neuroembryology. Specifically, we investigated the similarities of auditory neurons in nucleus magnocellularis (NM) and nucleus laminaris (NL). NM and NL comprise a well-described neural circuit in the auditory brainstem used to study binaural auditory processing, development (including circuit assembly), and afferent influence on neuronal death and dendrite dynamics (for reviews, see Rubel et al., 1990; Fritzsch et al., 2002; Burger and Rubel, 2008).

Abbreviations

4v	fourth ventricle
cc	central canal
D	dorsal
dh	dorsal horn
DL-APV	DL-2-amino-5-phosphonovaleric acid
DRG	dorsal root ganglion
DTX	dendrotoxin
E	embryonic day
Fl	flocculus
GFP	green fluorescent protein
NBQX	1,2,3,4-tetrahydro-6-nitro-2,3-dioxo-benzo[f]quinoxaline-7-sulfonamide disodium salt hydrate, FG 9202 disodium salt hydrate
NL	nucleus laminaris
NM	nucleus magnocellularis
NT	neural tube
P	postnatal day
PFA	paraformaldehyde
PFl	paraflocculus
PTX	picrotoxin
RT	room temperature
SGFS	stratum griseum et fibrosum superficilale
tect	tectum
TTX	tetrodotoxin
V	ventral
vh	ventral horn

We show that the structure and function of NM and NL neurons in the GFP quail are nearly identical to those of the chicken. These similarities suggest that transgenic quail are a viable alternative to the chicken model to study the avian nervous system, especially when transgenic quail lines are produced that manipulate the expression of specific genes and/or to identify specific neuronal types. We suggest that the GFP quail can be an advantageous model system to study the avian brain when readily labeled and highly identifiable neurons are desired.

MATERIALS AND METHODS

Animals

Fifty-one Japanese quail (Coturnix coturnix japonica) embryos and hatchlings (embryonic day [E]9–posthatch day [P]6) of either sex were used. The day of hatching was considered to be posthatch 0 (P0). Quail hatch at E16. In addition, 18 white Leghorn chicken (Gallus gallus domesticus) embryos and hatchlings (E11–P10) of either sex were used for comparison. Chickens hatch at E21.

All experimental methods and animal husbandry procedures to generate transgenic quail were carried out in accordance with the guidelines of the National Institutes of Health and with the approval of the Institutional Animal Care and Use Committee at the California Institute of Technology (Huss et al., 2008). All other surgical procedures were approved by the University of Washington Institutional Animal Care and Use Committee and conformed to NIH guidelines. All efforts were made to minimize pain or discomfort of the animals used and to minimize the number of the animals used.

Production of transgenic quail

Two lines of transgenic quail were produced and used in the current study. The first line is Tg(*syn1*:eGFP) transgenic quail that express eGFP driven by the human synapsin gene I promoter. The production of this line has been described before (Scott and Lois, 2005). The second line is Tg(*syn1*:H2B-eGFP) transgenic quail that express eGFP fused with a nuclear localized protein, histone H2B. The original vector pLenti.Syn(0.5):eGFP has been previously characterized (Dittgen et al., 2004). pLenti.Syn(0.5):eGFP was linearized with *Bam*H1 and *Age*1 and then ligated with a fragment containing *Bgl*2-*Age*1 H2B. The final plasmid vector, pLenti.Syn(0.5):H2B-eGFP (9,655 bp), was electroporated into *E. coli* DH10B (Invitrogen, Carlsburg, CA). Purified plasmid DNA was isolated from transformed *E. coli* by using standard column filter techniques (Qiagen, Valencia, CA).

Lentivirus production

293FT cells (Invitrogen) were grown on gelatin-coated plates and transfected with pLenti.Syn(0.5):H2B-eFFP by using Lipofectamine 2000 along with the ViraPower Lentiviral Packaging Mix (Invitrogen) according to the manufacturer's protocol. Supernatants were collected at 24, 48, and 72 hours post transfection, filtered at 0.45 μm, and stored at −80°C until concentration. Supernatants were concentrated by using Centricon Plus filter devices with a 30-kDa MW cutoff (Millipore, Billerica, MA) according to the manufacturer's protocol. The resulting supernatants were ultracentrifuged at 50,000*g* for 2 hours at 4°C. The lentiviral pellets were resuspended in DMEM (Mediatech, Manassas, VA) and stored at −80°C. The lentiviral titer was determined by infecting cells with serial dilutions of the concentrated virus.

Production and analysis of transgenic quail

The transgenic quail were produced by using previously published protocols (Sato et al., 2010) by the injection of concentrated lentivirus solution into the subgerminal cavity of stage X Japanese quail embryos (Eyal-Giladi and Kochav, 1975). One G0 mosaic founder was bred to a wild-type (WT) mate, which produced two transgenic offspring that were grown to adulthood and bred for experimental analysis. We screened G1 hatchlings for the presence of the transgene by using standard molecular techniques (Sambrook and Russell, 2001). First, polymerase chain reaction (PCR) analysis was performed on genomic DNA isolated from the chorioallantoic membrane (CAM) tissue of the eggshell after hatching. The CAM was scraped from the inside of the shell and digested overnight at 55°C in the presence of sodium dodecyl sulfate (SDS) and proteinase K. The genomic DNA was isolated by using standard phenol/chloroform extraction protocols. Genomic DNA (100 ng) was used to perform multiplex PCR with oligonucleotide primers designed against the H2B-eGFP portion of the transgene along with chicken GAPDH as a housekeeping control. Once transgenic birds had been identified, the number and uniqueness of transgene integrations was determined by using Southern blot analysis. Genomic DNA (5 μg) was digested with *Pst*I, separated on a 0.8% agarose gel, and transferred to a nylon membrane. The blot was hybridized with a 646-bp ^{32}P-labeled DNA probe against the woodchuck hepatitis virus posttranscriptional response element (Wpre) of the transgene.

Cochlea removal

A previously described procedure was used for cochlea ablation (Born and Rubel, 1985). Quail (P1–P6) were anesthetized with a mixture of 40 mg/kg ketamine and 12 mg/kg xylazine. A small incision was made to widen the external auditory meatus of the ear. The tympanic membrane and columella were removed to expose the oval window. The basilar papilla, including the lagena macula, was removed via the oval window using fine forceps, floated on water, and examined with a surgical microscope to verify complete removal. Only animals with a complete removal of the basilar papilla, including the lagena, were used for further tissue processing and data analysis. This procedure results in complete removal of the basilar papilla, but spares the ganglion cells. In total, 15 animals received a unilateral cochlea removal (right ear). Four were allowed to survive for 4 hours, four for 14 hours, four for 1 day, and three for 6 days. Four additional animals did not receive the surgery and served as controls.

Immunohistochemistry

Distribution and expression level of proteins of interest were examined by using peroxidase or fluorescent immunohistochemistry in control animals ($n = 9$) or those used for cochlea removal experiment ($n = 19$; Wang and Rubel, 2008). For embryos, quail were rapidly decapitated and the brains were removed from the skull and immersion-fixed overnight in 4% paraformaldehyde (PFA) in phosphate buffer (PB; 0.1 M, pH 7.4) at 4°C. For hatchlings, quail were anesthetized with a mixture of 200 mg/kg ketamine and 60 mg/kg xylazine and transcardially perfused with 0.9% saline followed by 4% PFA. The brain was removed from the skull and postfixed overnight in the same fixative. All embryo and hatchlings brains were then cut coronally either at 12 μm on a cryostat (Leica CM 1850, Leica Biosystems, Richmond, IL), at 30–40 μm on a freezing sliding microtome, or at 50 μm with a vibratome (Leica VT 1000S). Sucrose cryoprotection was applied prior to cryostat or microtome sectioning.

Sections were collected in phosphate-buffered saline (PBS; 0.01 M, pH 7.4) into alternate series, and stained for either Nissl substance or immunohistochemically for microtubule-associated protein 2 (MAP2), glutamate decarboxylase 65 (GAD65), gephyrin, and voltage-gated potassium channel 1.2 (Kv1.2). Free-floating sections were incubated with primary antibody solutions diluted in PBS with 0.3% Triton X-100 for 6 hours to overnight at 4°C, followed by biotinylated anti-IgG antibodies (1:200; Vector, Burlingame, CA) or AlexaFluor secondary antibodies (1:200–1:500; Molecular Probes, Eugene, OR) for 1–4 hours at room temperature (RT).

For peroxidase immunohistochemical staining, sections were incubated in avidin–biotin–peroxidase complex solution (ABC Elite kit; Vector) diluted 1:100 in PBS with 0.3% Triton X-100 for 1 hour at RT. Sections were incubated for 3–7 minutes in 0.015% 3-3′-diaminobenzidine (Sigma-Aldrich, St. Louis, MO), either with 0.01%

TABLE 1.
Primary Antibodies Used

Antigen	Immunogen	Manufacturer, species antibody was raised in; mono- vs. polyclonal; cat. and lot nos.	Dilution
Microtubulin-associated protein 2 (MAP2)	Bovine brain MAP2 (amino acids 997–1,332)	Chemicon; mouse; monoclonal; clone AP20; MAB3418; lot LV1486526	1:1,000
Glutamate decarboxylase 65 (GAD65)	Human GAD65 from baculovirus-infected cells	Millipore; rabbit; polyclonal; AB5082; lot LV1580833	1:1,000
Gephyrin	Purified rat gephyrin	Synaptic Systems; mouse; monoclonal, clone mAB7a; 147011; lot 147011/21	1:1,000
Potassium channel 1.2 (Kv1.2)	Fusion protein of rat Kv1.2 (amino acids 428–499; cytoplasmic C-terminus)	NeuroMab; mouse; monoclonal; clone K14/16;	1:1,000
Class III β-tubulin	Rat brain microtubules	Covance, mouse monoclonal, clone: TUJ1, cat no: MMS-435P, lot no.: 14920201.	1:1,000

hydrogen peroxide in PBS or with 0.03% hydrogen peroxide, 125 mM sodium acetate, 10 mM imidazole, and 100 mM nickel ammonium sulfate. Sections were mounted on gelatin-coated slides and then dehydrated, cleared, and coverslipped with DPX mounting medium (EMS, Hatfield, PA). For fluorescent immunocytochemical staining, sections were mounted and coverslipped with either Fluoromount-G (SouthernBiotech, Birmingham, AL), Glycergel (Dako, Carpinteria, CA), or Vectashield (Vector).

Antibody characterization

The immunogen, clone type, and manufacturer's information, as well as dilution used for each antibody, are provided in Table 1. Specificity of antibodies for MAP2, GAD65, and gephyrin in chicken brain tissue has been described in previous studies from our laboratory (Wang et al., 2009; Tabor et al., 2011). Briefly, anti-MAP2 binds specifically to MAP2a and MAP2b and is detected as a 300-kDa band in western blot analysis. Anti-GAD65 reacts strongly with GAD65-containing nerve terminals and recognizes a 65-kDa protein corresponding to GAD65 by western blot of mouse brain extract. Anti-gephyrin stains the brain-specific 93-kDa splice variant and was shown to detect the N-terminus of gephyrin in western blot (Pfeiffer et al., 1984). The staining pattern revealed in the current study for each of these antibodies is identical to that of published studies.

According to the manufacturer's information, anti-Kv1.2 does not cross-react with Kv1.1, Kv 1.3, Kv1.4, Kv1.5, or Kv 1.6 expressed in transfected cells. It detects a molecular weight at 80 kDa in brain membranes prepared from WT mice or rat, which is absent from Kv1.2 knockout mice.

Electrophysiology

Acute brainstem slices were prepared from transgenic quail (E14–16) and chicken (E19–21) as described previously (Sanchez et al., 2010). Briefly, bilaterally symmetrical coronal slices were made (200–300 μm thick) from the rostral one-half of NL and collected in normal artificial cerebrospinal fluid (ACSF) containing the following (in mM): 130 NaCl, 3 KCl, 1.25 NaH_2PO_4, 26 $NaHCO_3$, 1 $MgCl_2$, 3 $CaCl_2$, and 10 glucose, pH adjusted to 7.3 with KOH

TABLE 2.
Animal Ages by Experiment

Experiment	Method	Age
GFP expression	Unstained sections	E9, E11, E14, P5
Cytoarchitecture	MAP2 IHC	P1–P6
Calyx of Held	Dye electroporation	P2–P5
NM axon	Dye electroporation	E14
Inhibitory terminal on NL	GAD65 & gephyrin IHC	E14
Kv1.2 channel expression	Kv1.2 IHC	E14
Intrinsic and synaptic properties	In vitro whole-cell patch clamp physiology	E14–16
Afferent influences	Cochlea removal MAP2 IHC	P1–P6

Abbreviations: GAD65, glutamate decarboxylase 65; GFP, green fluorescent protein; IHC, immunohistochemistry; MAP2, microtubule-associated protein 2.

Voltage-clamp and current-clamp experiments were performed by using an Axon Multiclamp 700B amplifier (Molecular Devices, Sunnyvale, CA). Patch pipettes were pulled to a tip diameter of 1–2 μm and had resistances ranging from 3 to 6 MΩ. For voltage-clamp experiments, the internal solution was cesium-based containing the following (in mM): 108 $CsMeSO_3$, 5 CsCl, 1 $MgCl_2$, 15 phosphocreatine-$Tris_2$, 8 BAPTA-Cs_4, 10 HEPES, 3 QX-314.Cl, 4 MgATP, 0.4 $Tris_2GTP$, pH adjusted to 7.3 with TrisOH. The liquid junction potential was 5 mV, and data were adjusted accordingly. The cesium-based internal solution was used to block K^+ conductances and QX-314 chloride

was used to block Na^+ conductances in an attempt to reduce space-clamp issues associated with dendritic filtering. Series resistance was compensated for by ~80% in all voltage-clamp recordings. For current-clamp experiments, the internal solution was potassium-based containing the following (in mM): 105 K-gluconate, 35 KCl, 1 $MgCl_2$, 10 HEPES-K^+, 5 EGTA, 4ATP-Mg^{2+}, and 0.3 GTP-Na^+, pH adjusted to 7.3 with KOH. The liquid junction potential was 10 mV, and data were adjusted accordingly.

A small hyperpolarizing (−1 mV, 100 ms) voltage command was presented at the beginning of each recorded trace to document and monitor whole-cell parameters (resting membrane potential [RMP], cell membrane capacitance, series resistance, and input resistance). RMPs were measured immediately after break-in to avoid cesium-induced depolarization during voltage-clamp experiments. Neurons were included in the data analysis only if they had RMPs between −50 mV and −65 mV and had series resistances <15 MΩ. Raw data were low-pass-filtered at 2 kHz and digitized at 10 kHz by using a Digidata 1440A (Molecular Devices).

Pipettes were visually guided to NL and neurons were identified and distinguished from surrounding tissue based on cell morphology, known laminar structure, and location of the nucleus within the slice. All experiments were conducted in the presence of the γ-aminobutyric acid A receptor ($GABA_A$-R) antagonist picrotoxin (PTX, 100 μM). After a GΩ seal was attained, membrane patches were ruptured and NL neurons were held in whole-cell configuration for voltage-clamp recording at the following membrane potentials: −60 mV for isolated AMPA-R–mediated excitatory postsynaptic currents (EPSCs); −80 mV for isolated AMPA-R–mediated EPSC depression; and −60 mV for isolated K^+ currents (voltage-clamp).

For current-clamp experiments, NL neurons were held in whole-cell configuration at I = 0 for recording intrinsic and synaptic membrane potentials. Isolated AMPA-R–mediated EPSCs were recorded in the presence of an N-methyl-D-aspartate receptor (NMDA-R) antagonist, DL-2-amino-5-phosphonopentanoic acid (DL-APV; 100 μM). Isolated K^+ currents were recorded in the presence of the Na^+ blocker tetrodotoxin (TTX; 1 μM), the AMPA-R antagonist 1,2,3,4-tetrahydro-6-nitro-2,3-dioxo-benzo[f]-quinoxaline-7-sulfonamide disodium salt hydrate (NBQX; 20 μM), and DL-2-amino-5-phosphonovaleric acid (DL-APV). Dendrotoxin (DTX-I; 0.1 μM) and fluoxetine (100 μM) were used to selectively block low- and high-voltage activated K^+ currents, respectively. K^+ leak currents were subtracted offline by using the responses to the hyperpolarizing steps from −80 to −90 mV as a baseline.

Extracellular synaptic stimulation was accomplished by using a concentric bipolar electrode (tip core diameter: 200 μm; World Precision Instruments, Sarasota FL). Square electric pulses, 100 μs in duration, were delivered by an Iso-flux stimulator (A.M.P.I; Jerusalem, Israel) and interval generator (S88; Grass, West Warwick, RI). Stimulating electrodes were placed in the dorsal neuropil region of NL, approximately 30–50 μm from recorded NL neurons. For current–voltage (I–V) experiments of isolated AMPA-R currents, spermine (100 μM; N,N-bis(3-aminopropyl)-1,4-diaminobutane, gerontine, musculamine, neuridine) was added to the internal pipette solution to reduce dialyzation of endogenous polyamines. Spermine is a polyamine that blocks ion flux in a voltage-dependent manner for AMPA-Rs lacking the GluA2 subunit.

Recording protocols were written and run by using Clampex acquisition and Clampfit analysis software (version 10.1; Molecular Devices). Statistical analyses and graphing protocols were performed by using Prism (version 5.0a; GraphPad, La Jolla, CA). The standard for significant differences was defined as $P < 0.05$.

All bath-applied drugs were allowed to perfuse through the recording chamber for 2 minutes before subsequent recordings. D-APV, NBQX, spermine, and all other salts and chemicals were obtained from Sigma-Aldrich. DTX-I, PTX, and fluoxetine were obtained from Tocris (Ellisville, MO). TTX and QX-314 were obtained from Alomone Labs (Jerusalem, Israel).

Axon labeling

Terminal morphology and projection pattern of the auditory nerve and NM axons were examined by electroporation of a fluorescent dextran dye into a small number of the auditory (eighth) nerve axons or a small cluster of NM cells in GFP quail (E14–P6) and chickens (E20), as described previously (Burger et al., 2005; Seidl et al., 2010). Briefly, the whole brainstem blocks or thick slices (1,000 μm) that contain NM and NL were prepared as described above for physiological recordings. Alexa Fluor 568 dextran (20 mM in sterile 0.9% saline; Invitrogen) was electroporated with square voltage pulses (100 μs) applied through a glass pipette with a tip diameter of 1–2 μm. Following electroporation, the tissues were returned to oxygenated ACSF for additional 4 hours at RT followed by fixation in 4% PFA for 1–4 hours. To observe the terminal morphology of the auditory nerve within NM, the brainstem was sectioned at 100 μm by using a vibratome before coverslipping. For projection pattern of NM axons, the 1,000-μm-thick slices were dehydrated in a series of ethanol steps and put into a clearing solution (3:5 mixture of benzyl benzoate and methyl salicylate), so that filled

cells and axons could be imaged in their entirety in these 1,000-μm tissue slabs.

Imaging

eGFP, filled neuronal structure, and immunoreactivity were imaged by using confocal microscopy (FluoView FV1000 or FluoView FV300, Olympus, Tokyo, Japan). Acquired images were false-colored in Adobe Photoshop (Adobe Systems, San Jose, CA). All images are shown in the coronal plane and dorsal is up.

RESULTS

The brainstem auditory nuclei of the developing chicken embryo and hatchling have been studied extensively (for reviews, see Rubel et al., 1990; Kubke and Carr, 2000; Fritzsch et al., 2002; Hyson, 2005; Burger et al., 2011). Here we repeated several anatomical, biochemical, and biophysical studies previously done in chickens with the Tg(*syn1*:eGFP) and Tg(*syn1*:H2B-eGFP) quail, (collectively referred to as GFP quail) to

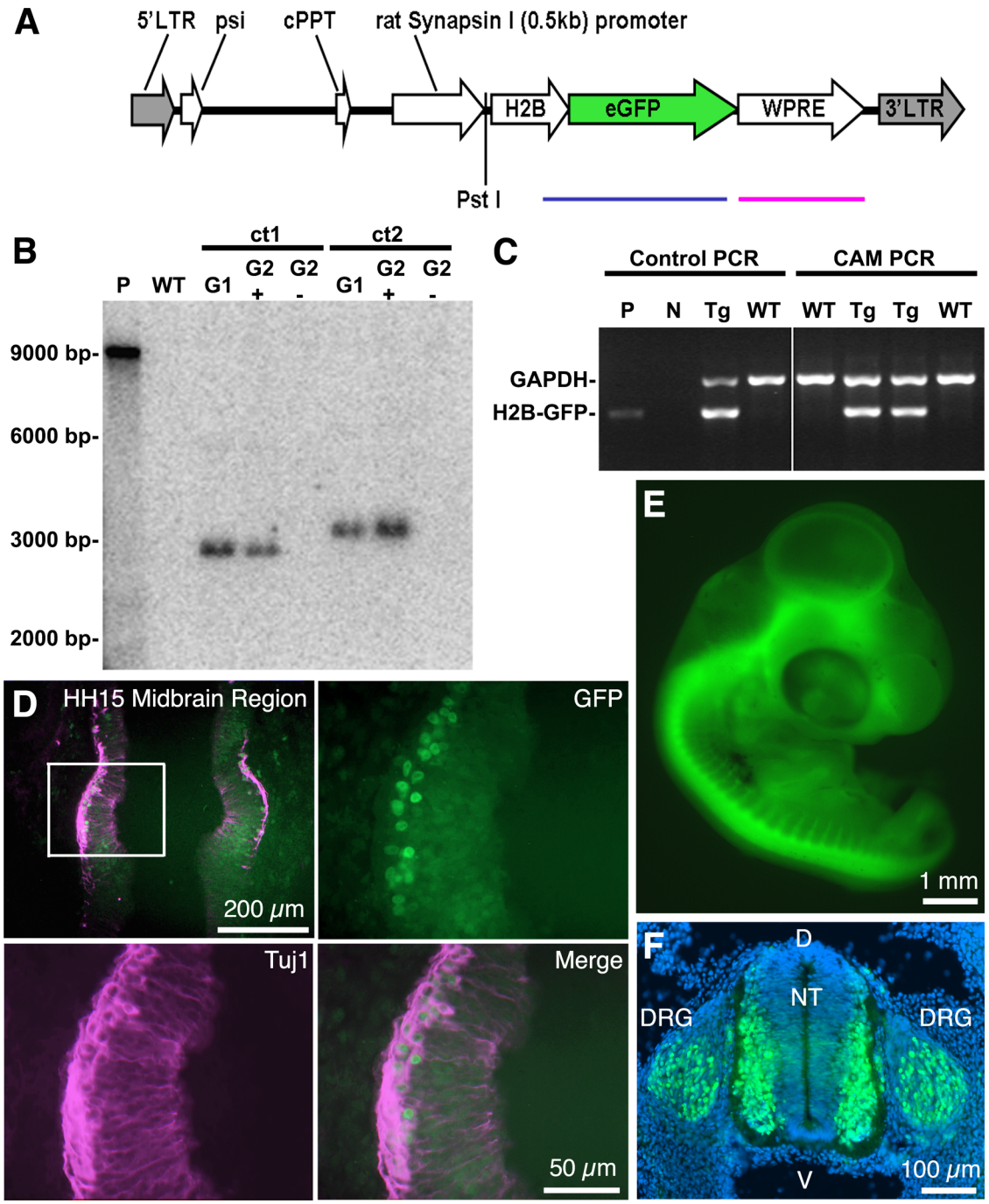

Figure 1

demonstrate similarities in auditory brainstem structure and function between the chicken and GFP quail.

Neuronal eGFP transgenic quail

HIV based VSV-g pseudotyped lentiviruses were used to produce two transgenic quail expressing eGFP under the control of the synapsin promoter: Tg(*syn1*:eGFP) quail expressed eGFP throughout the cytoplasm of neurons, whereas Tg(*syn1*:H2B-eGFP) quail expressed eGFP fused with a nuclear localized protein, histone H2B (Fig. 1A–C). Expression of eGFP was first observed at Hamburger–Hamilton (HH) stage 15 (E3) in the differentiating neurons within the midbrain anlage concomitant with the onset of synapsin mRNA expression (Fig. 1D). Both Tg(*syn1*:eGFP) and Tg(*syn1*:H2B-eGFP) quail lines fluorescently marked neurons throughout the brain and spinal cord in a specific and heritable manner during embryonic development (Fig. 1E,F) and after hatching (Fig. 2A–L).

Expression of eGFP in the developing auditory brainstem

Figure 3 shows eGFP expression in NM and NL neurons of the Tg(*syn1*:eGFP) quail at E9, E11, E14, and P5. At all ages examined, neurons of NM and NL formed distinct nuclei. NM neurons had round somas with no visible dendrites (Fig. 3A–D). In contrast, NL, positioned ventrolateral to NM (Rubel et al., 1976; Jhaveri and Morest, 1982; Young and Rubel, 1983), was composed of neurons arranged in a monolayer with bipolar dendrites extending dorsally and ventrally (Fig. 3A–F), similar to the anatomy of the chicken NL (Smith and Rubel, 1979).

Anatomy and morphology of NL and NM in GFP quail resemble chicken counterparts

We examined the detailed morphology of NL neurons by using immunohistochemistry for MAP2, a universal somatodendritic marker (Matus et al., 1981) previously used to study the chicken auditory brainstem (Wang and Rubel, 2008). MAP2 immunolabeling of P3 GFP quail brainstems confirmed that NM neurons had round cell bodies that were usually devoid of dendrites (Fig. 4A,B) and that bipolar NL neurons were arranged in a monolayer with dorsal and ventral dendritic domains (Fig. 4C–E). The length and complexity of NL dendritic arbors increased dramatically from rostromedial to caudolateral (Fig. 4CE), resembling the pattern of NL dendrites along the tonotopic axis in late embryonic and posthatch chickens (Smith and Rubel, 1979; Smith, 1981; Wang and Rubel, 2008).

A striking feature of the chicken auditory brainstem is the large, calycine terminals (endbulbs of Held) formed by the auditory nerve terminals on NM cell bodies (Jhaveri and Morest, 1982). To examine the morphology of auditory nerve terminals in GFP quail, we labeled individual axons using dye electroporation. In both Tg(*syn1*:eGFP) and Tg(*syn1*:H2B-eGFP) quail (P5 and P2, respectively) the endbulbs appeared similar in morphology to the endbulbs of Held found in E20 chicken embryos (data not shown) and hatchlings (Parks and Rubel, 1978; Jhaveri and Morest, 1982) (Fig. 5A–C).

The NM axon projection to NL in GFP quail mirrors the chicken anatomy. In GFP quail, fluorescently labeled NM axons projected to the ipsilateral and contralateral NL (Fig. 6A). Contralaterally extending axons traversed the

Figure 1. Characterization of Tg(*syn1*:H2B-eGFP) embryonic quail. **A:** Schematic representation of the *syn1*:H2B-eGFP lentivector following chromosomal integration. The length of the proviral sequence from the 5′ LTR to the 3′ LTR is 4,810 bp. The blue line indicates the 859-bp sequence spanning the H2B and eGFP regions amplified by PCR for genotyping. The red line indicates the region of the transgene sequence identified by a 646-bp probe used for Southern blotting. The *Pst*I restriction site used to digest the genomic DNA for Southern blotting analysis is indicated. LTR, long terminal repeat; psi, packaging signal; cPPT, central polypurine tract; H2B, histone 2B; WPRE, woodchuck hepatitis virus posttranslational regulatory element. **B:** Southern blot analysis of genomic DNA isolated from the chorioallantoic membrane (CAM) of eggshells after hatching. The blot shows two positive G_1 hatchlings: Tg(*syn1*:H2B-eGFP)^{ct1} and Tg(*syn1*:H2B-eGFP)^{ct2} (ct, Caltech). Both lines show single transgene integrations at distinct sites within the genome of the hatchlings (ct1, 2,900 bp; ct2, 3,200 bp). When bred to a WT, these G_1 birds produced phenotypically positive G_2 hatchlings ($G2^+$) about 50% of the time, as expected. Phenotypically negative G_2 hatchlings ($G2^-$) lacked the transgene, as did known wild-type hatchlings (WT). P, plasmid DNA control, 9,655 bp. **C:** Screening of hatchling genomic DNA for Tg(*syn1*:H2B-eGFP). Multiplex PCR was performed by using chicken glyceraldehyde 3-phosphate dehydrogenase (GAPDH; 1,445 bp) as a housekeeping control. Oligonucleotide primers amplified an H2B-eGFP fragment of 859 bp in transgenic animals. Two positive Tg and two negative WT are shown. Controls: P, plasmid DNA; N, no gDNA control; Tg, known transgenic gDNA; WT, known wild-type gDNA. **D:** Transgene expression is first detected in the midbrain region of stage HH15 quail embryos. HH15 Tg(*syn1*:H2B-eGFP) embryos were fixed, cryosectioned, immunolabeled with antibodies against β-III tubulin (Tuj1, red), and counterstained with DAPI (blue). GFP-positive nuclei (green) are colocalized with cells positive for the neural specific marker. Highlighted rectangular region in the upper left panel shown at higher magnification in upper right and lower panels. **E:** Neural specific eGFP expression continues throughout embryonic development. Wholemount E4 Tg(*syn1*:H2B-eGFP) embryo showing eGFP expression throughout the CNS. **F:** Transverse section through an E4 Tg(*syn1*:H2B-eGFP) embryo showing strong eGFP expression in the dorsal root ganglion (DRG) and the lateral aspects of the neural tube (NT). D, dorsal; V, ventral. Scale bar = 200 μm in D, upper left; 50 μm in D, lower right (also applies to upper right and lower left); 1 mm in E; 100 μm in F.

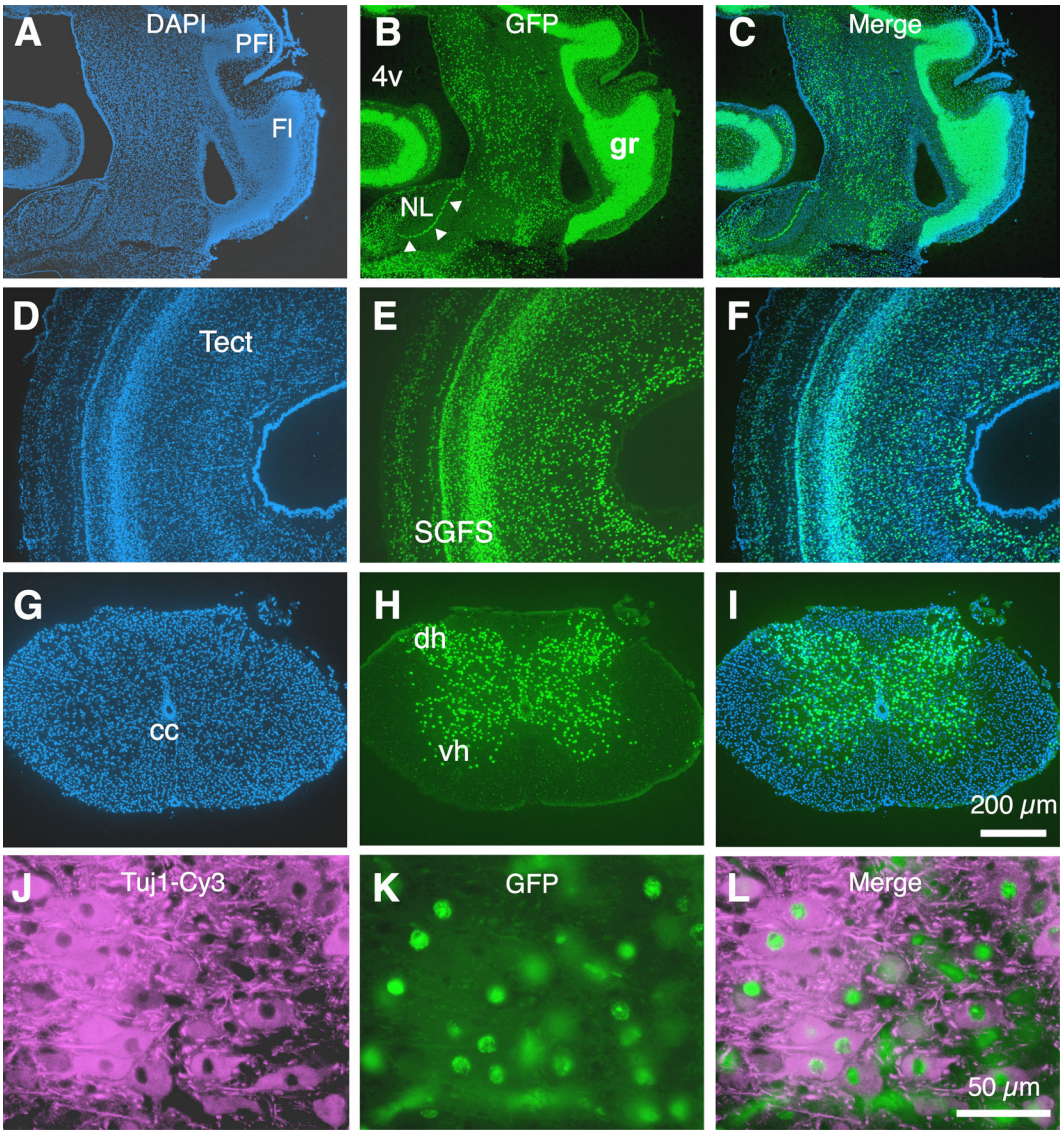

Figure 2. Characterization of Tg(*syn1*:H2B-eGFP) post-hatch quail. **A-C** (DAPI, eGFP, merge, respectively): Neural-specific eGFP expression continues after embryonic development. A section of a P1 Tg(*syn1*:H2B-eGFP) quail containing nucleus laminaris (arrowheads in B.). The granule cell layer of the cerebellum (gr in B), with its dense layer of cell nuclei, is highly labeled. DAPI counterstain, blue. PFl, paraflocculus; Fl, flocculus; NL, nucleus laminaris; 4v, fourth ventricle. **D–F:** All regions of the brain show neural-specific eGFP expression. A section through the optic tectum of a P1 Tg(*syn1*:H2B-eGFP) quail. The various tissue layers within the stratum griseum et fibrosum superficilale (SGFS) of the tectum (tect) are clearly visible. **G–I:** Transverse section of the spinal cord of a P1 Tg(*syn1*:H2B-eGFP) quail showing eGFP-positive nuclei localized to the gray matter of the maturing neural tissue. cc, central canal; dh, dorsal horn; vh, ventral horn. **J–L:** P1 Tg(*syn1*:H2B-eGFP) spinal cord section immunolabeled with antibodies against β-III tubulin (Tuj1, red). GFP-positive nuclei (green) are colocalized with cells positive for the neural-specific marker. Scale bar = 200 μm in I (applies to A–I); 50 μm in L (applies to J–L).

midline just ventral to the fourth ventricle, before they terminated on the ventral dendrites of the contralateral NL (Fig. 6A,B). Ipsilateral axons projected to the dorsal dendritic domain of the ipsilateral NL (Fig. 6C). As in chickens, contralateral and ipsilateral NM terminal axons were restricted to either the ventral or dorsal dendrites, respectively, and only a few fibers crossed to the other side (Fig. 6B,C).

Immunolabeling patterns in GFP quail auditory brainstem

Studies in the chicken auditory brainstem have found several molecules with intriguing distribution patterns suggesting they play important roles in development and function (e.g., GABAergic synapse and voltage-dependent K^+ channels) of NM and NL. We examined the immunolabeling patterns of these molecules in GFP quail to

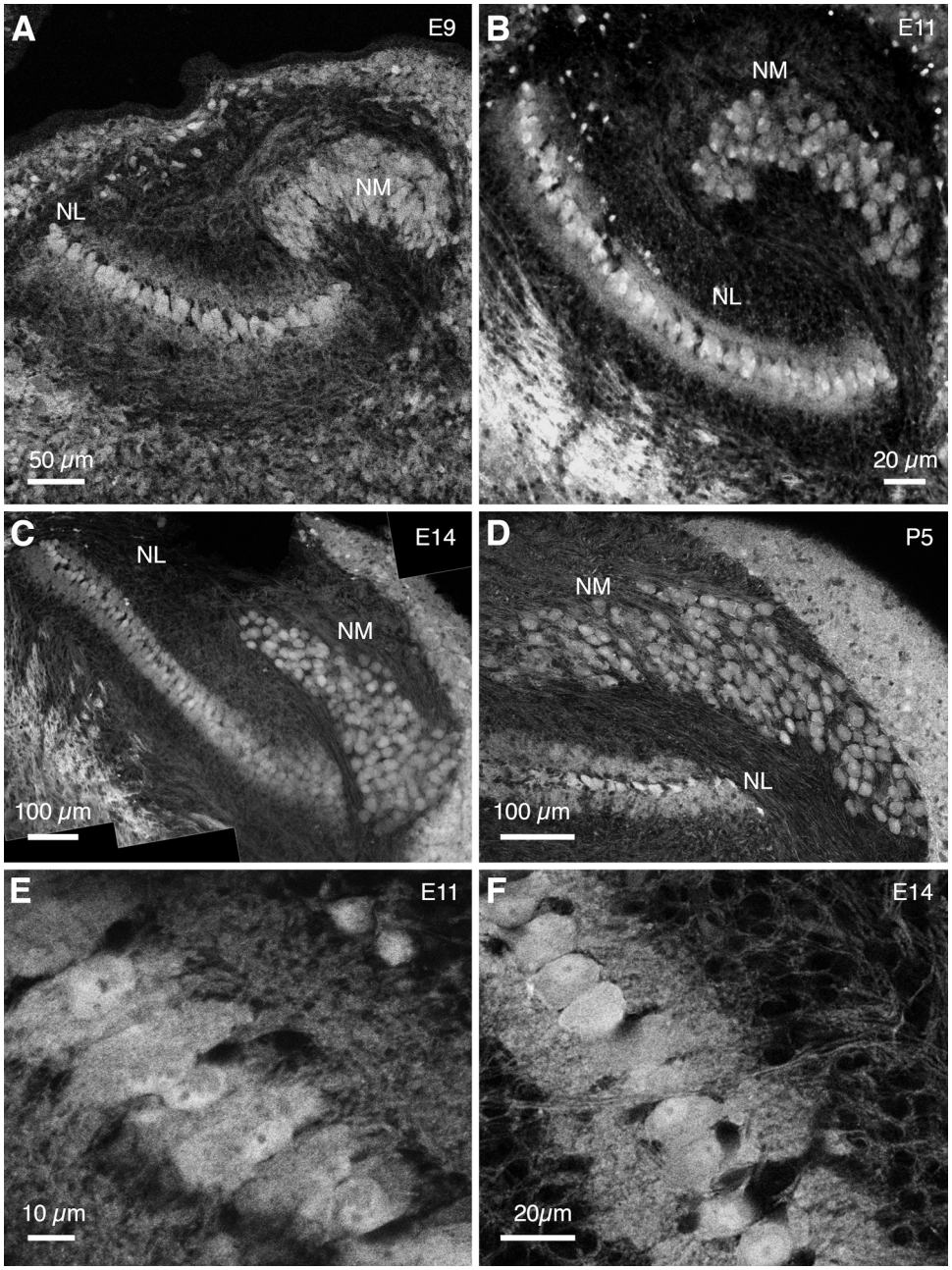

Figure 3. eGFP expression in auditory brainstem of Tg(*syn1*:eGFP) quail. **A–D:** At E9, E11, E14, and P5 eGFP is expressed in soma and dendrites of NM and NL neurons. At E9, nucleus magnocellularis (NM) and nucleus laminaris (NL) neurons are already distinct structures showing relatively mature configurations (A). At P5 NM neurons appear round, almost devoid of dendrites (D). **E,F:** eGFP expression in NL neurons reveals the monolayer organization of cell bodies and bipolar dendritic arbors. All images are coronal views, with dorsal up. Scale bar = 50 μm in A; 20 μm in B,F; 100 μm in C,D; 10 μm in E.

explore whether these molecules show similar distribution patterns in the NM-NL circuit.

GABAergic synapses in NL and NM

The distribution pattern of inhibitory synapses across NM and NL in E15 GFP quail was examined by using antibodies against GABAergic presynaptic (GAD65) and inhibitory postsynaptic (gephyrin) molecules. Figure 7A shows gephyrin immunolabeling, indicating inhibitory postsynaptic sites in NM and NL. Punctate immunostaining against GAD65 and gephyrin was observed surrounding NM cell bodies (Fig. 7B–D) and throughout the dendritic and neuronal domains of NL (Fig. 7E–G). Immunolabeled puncta were distributed across the tonotopic axis in both NM and NL (data not shown). The distribution pattern of inhibitory synapses was similar to the pattern observed in

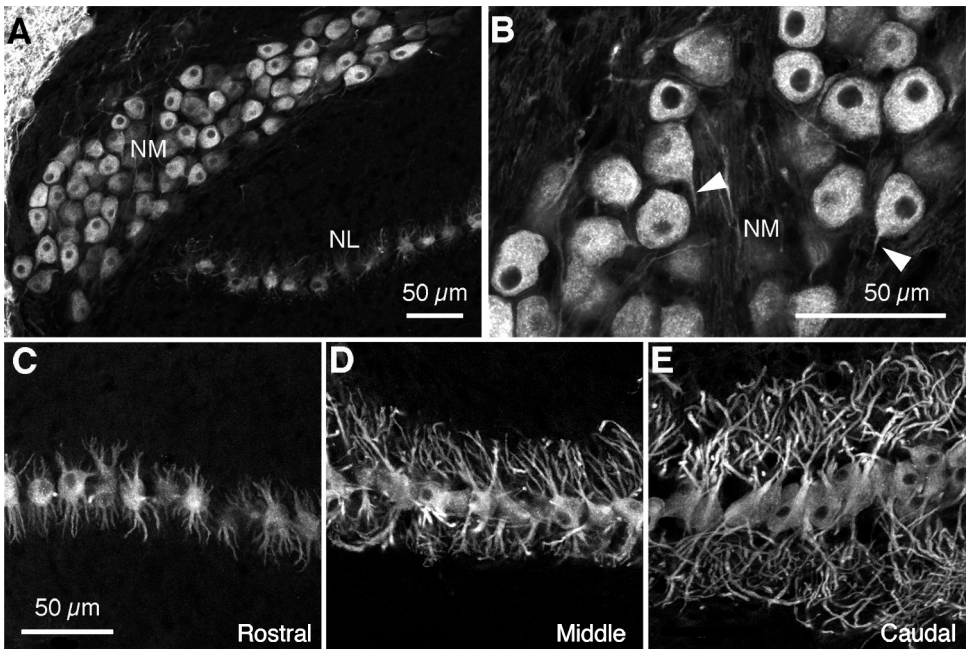

Figure 4. Nucleus magnocellularis (NM) and nucleus laminaris (NL) cytoarchitecture in post-hatch GFP quail. **A,B:** At P3 in GFP quail, similar to stage matched chickens, MAP2 immunoreactivity shows that NM neurons have round somata and very short processes are stained (white arrowheads in B). **C–E:** NL neurons show typical bipolar configuration with symmetric dorsal (up) and ventral (down) dendritic domains. From the rostromedial to the caudolateral poles of NL there is a gradient of increasing dendritic length along the tonotopic axis. Scale bar = 50 μm in A–C (that in C also applies to D,E).

chicken using the same antibodies (Tabor et al., 2011) and antibodies against other GABAergic synaptic components (vesicular GABA transporter [VGAT]: Nishino et al., 2008; GABA: Code et al., 1989; Kuo et al., 2009; $GABA_A$ receptors: Code and Churchill, 1991).

Kv1.2 channels in NL and NM

Spatial distribution of Kv1.2, a low-voltage activated potassium channel (K_{LVA}), was found in NL by immunostaining GFP quail brainstem sections at E14 (Fig. 8). High-magnification images revealed a high intensity of Kv1.2 immunolabeling at the proximal axon of NL neurons (Fig. 8A, arrowheads), resembling the pattern of Kv1.2 immunolabeling in the chicken auditory brainstem at E19 (Sanchez et al., in press).

Intrinsic physiological properties of NL neurons in GFP quail and chicken

Membrane responses of NL neurons

Current-clamp studies were performed on NL neurons from GFP quail (E14–16) and chicken (E19–21) by using hyperpolarizing and depolarizing current steps. Representative changes in membrane potentials are shown for E16 GFP quail NL neurons in Figure 9. In all neurons tested, only a single action potential (AP) occurred, despite large systematic increases in depolarizing current injections (Fig. 9A). In addition, voltage sag occurred in response to large negative current injections in both GFP quail and chicken (Fig. 9A). Voltage–current (V–I) relationships were constructed by measuring the steady-state membrane voltage after injection of current into the soma of NL neurons. The flattened V–I curves above the resting membrane potentials of the neurons were similar between GFP quail and chicken (Fig. 9B), indicating low input resistances.

K^+ conductances of NL neurons

K^+ conductances in voltage-clamped NL neurons from GFP quail (E14–16) and chicken (E19–21) were recorded while neurons were clamped at different holding potentials. Representative changes in K^+ currents from an E15 GFP quail NL neuron are shown in Figure 9C. I–V relationships were constructed by measuring the steady-state current response at different holding voltages (Fig. 9D). The I–V curves for both GFP quail and chicken NL neurons, showed that: 1) depolarizing voltage steps greater than −60 mV activated significant K_{LVA} currents; and 2) depolarizing voltage steps between −30 and +20 mV activated significant high-voltage activated potassium channel (K_{HVA}) currents (Fig. 9D). Indeed, these K^+ currents were highly sensitive to bath application of blockers of K_{LVA} (DTX-I) and K_{HVA} (fluoxetine) channels (data not shown). Hence, GFP quail NL neurons express strong K^+ conductances consisting of both K_{LVA} and K_{HVA} channels commonly found in age-equivalent chicken embryos.

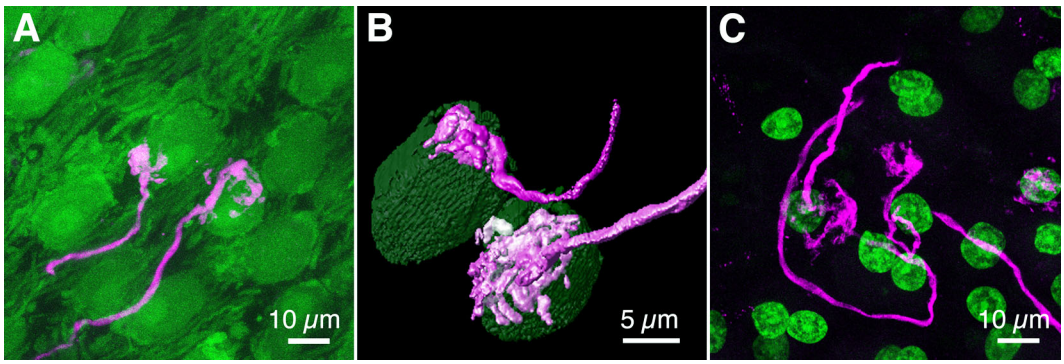

Figure 5. Calyx-type auditory nerve terminals in NM. **A:** Auditory nerve terminals on NM cell bodies in P5 Tg(*syn1*:eGFP) quail. **B:** 3D rendering of calyces and associated NM cells. **C:** Color-merged maximum intensity projection of NM in P2 Tg(*syn1*:H2B-eGFP) quail following dye electroporation into the auditory nerve. eGFP, green; dye, magenta. Scale bar = 10 μm in A,C; 5 μm in B.

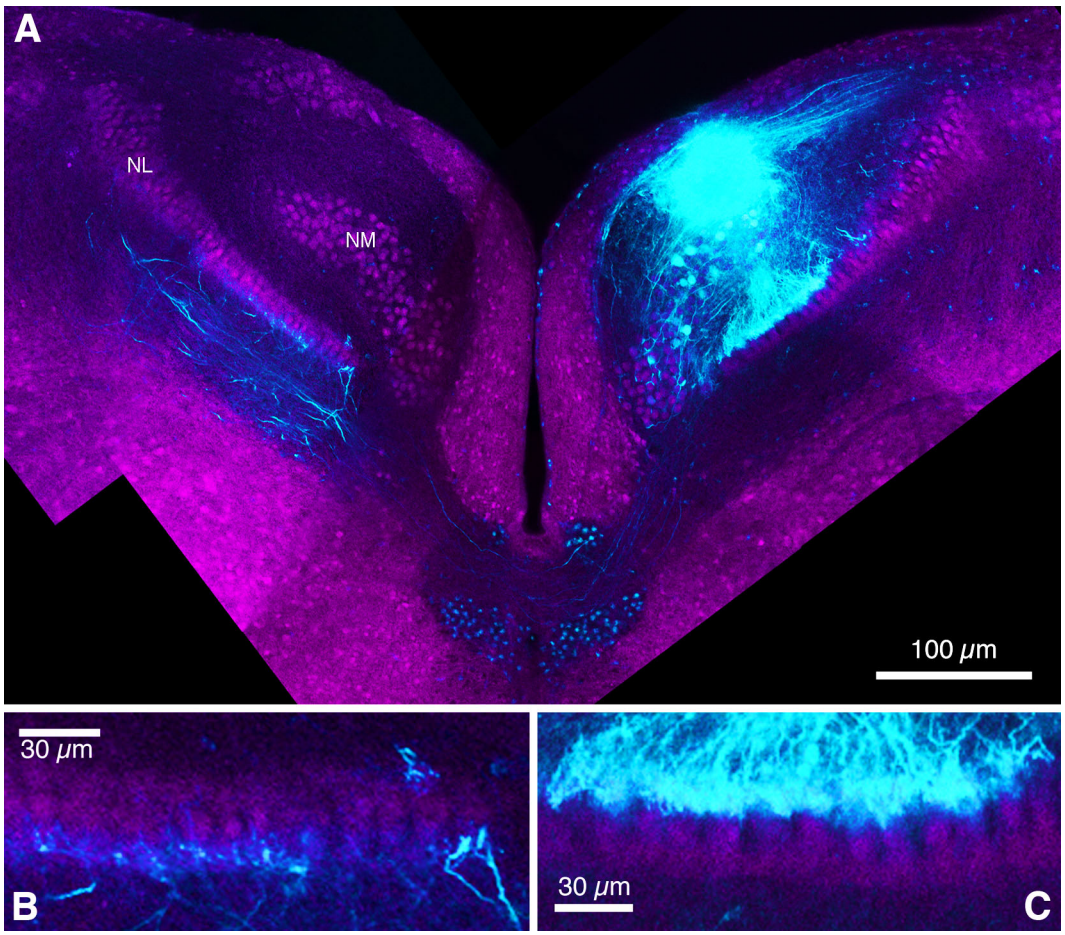

Figure 6. Nucleus magnocellularis (NM) axon projection pattern. **A:** NM axons send bilateral projections to neurons in nucleus laminaris (NL). The ipsilateral NM axon provides an input to the dorsal dendrites of NL neurons. The contralateral axons cross the midline and travel on the ventral side of NL neurons. **B:** Contralateral NM axons project to the ventral side of NL and very few axon fibers cross over to the dorsal neuropil. **C:** Ipsilateral axons project almost exclusively to the dorsal side of the ipsilateral NL neurons. eGFP, magenta; dye, cyan. Scale bar = 100 μm in A; 30 μm in B,C.

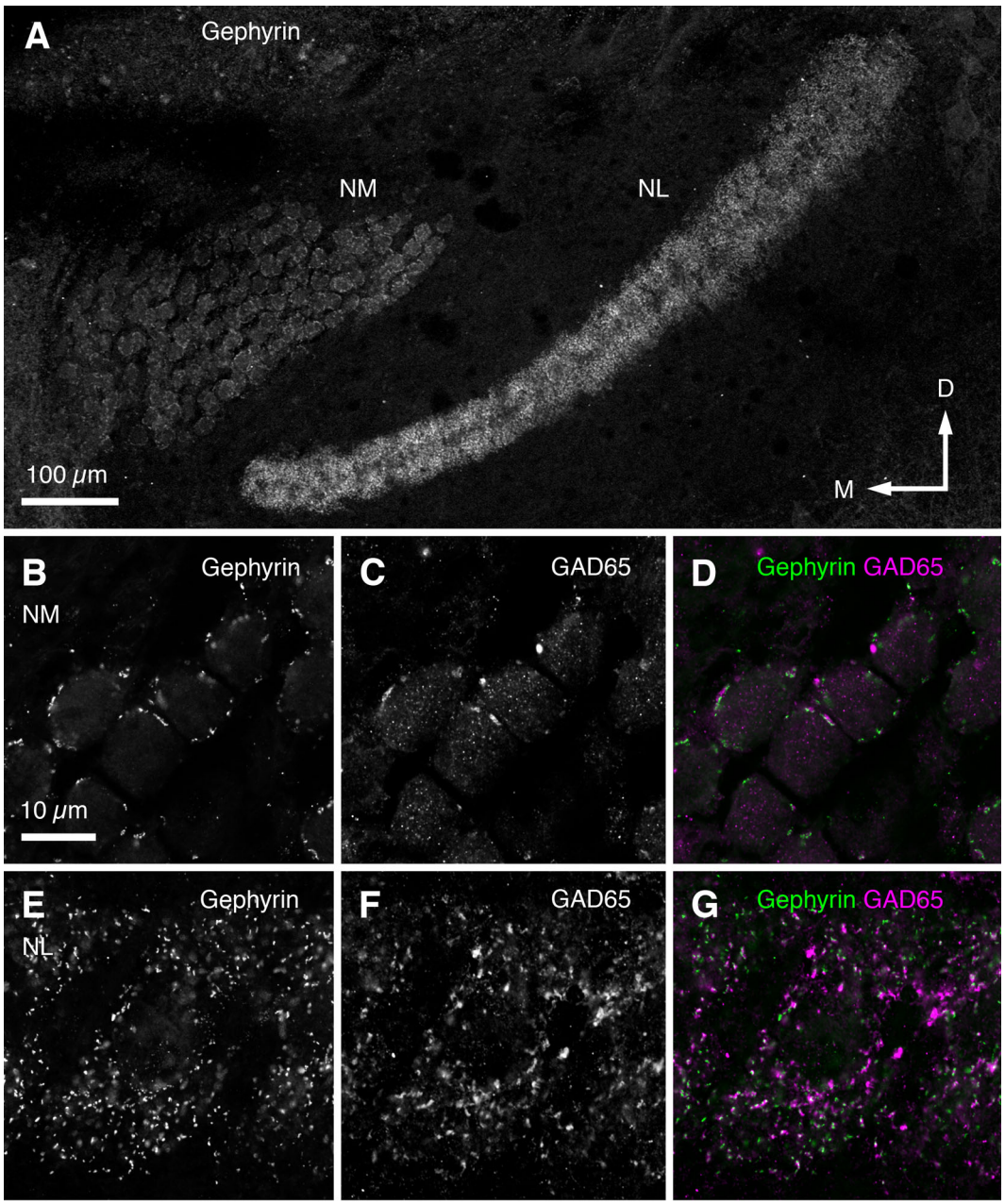

Figure 7. Pattern of inhibitory synapse distribution in nucleus magnocellularis (NM) and nucleus laminaris (NL). **A:** Gephyrin immunolabeling of inhibitory postsynaptic sites in NM and NL of E14 Tg(*syn1*:eGFP) quail. **B–D:** High-magnification images of gephyrin (B), GAD65 (GABAergic presynaptic sites; C), and combined (D) immunolabeling in NM. **E–G:** High-magnification images of gephyrin (E), GAD65 (F), and combined (G) immunolabeling in NL. Scale bar = 100 μm in A; 10 μm in B (applies to B–G).

Synaptic physiological properties of NL neurons in GFP quail and chicken

AMPA-R–mediated EPSCs of NL neurons

To determine whether EPSCs in the GFP quail NL neurons are mediated by rapid, subunit-specific AMPA-Rs, isolated AMPA-R–mediated EPSCs were recorded while NM inputs were electrically stimulated. Our results showed large, rapid, and highly consistent inward currents when GFP quail NL neurons were voltage-clamped at −60 mV. Example traces are superimposed and shown in Figure 10A from an E14 GFP quail NL neuron. The AMPA-R–mediated EPSC kinetics (rise time and decay tau) were extremely rapid and comparable to those recorded from age-equivalent chicken NL neurons (GFP quail rise: 0.44 ± 0.10 ms, chicken rise: 0.49 ± 0.07 ms; GFP quail decay: 0.73 ± 0.12 ms, chicken decay: 0.79 ± 0.14 ms; Fig. 10B). These currents were reversibly blocked by the AMPA-R antagonist NBQX (data not

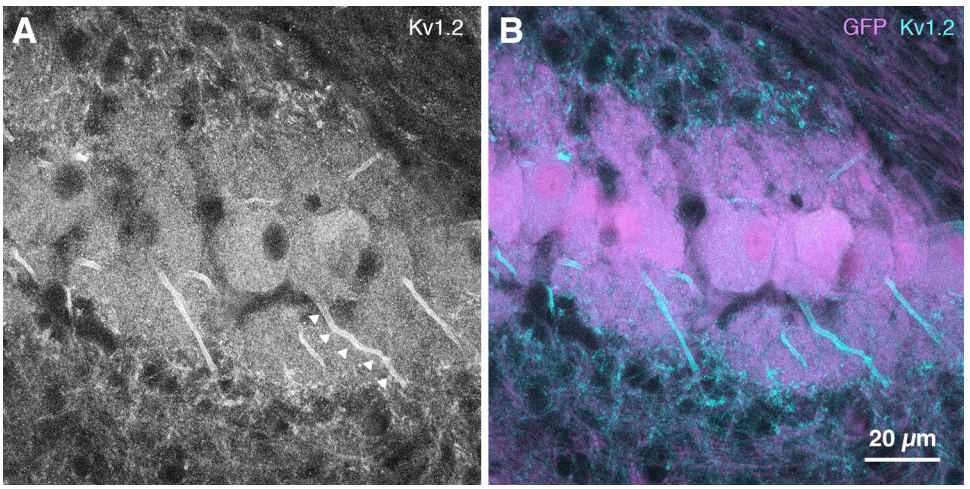

Figure 8. Kv1.2 immunohistochemistry in NL. **A,B:** Kv1.2 channel immunolabeling can be seen in the proximal axon, possibly indicating expression along the axon initial segment (arrowheads in A). eGFP, magenta; Kv1.2, cyan. Scale bar = 20 μm in B (applies to A,B).

shown), suggesting that inward current responses are mediated by AMPA-Rs in GFP quail NL neurons.

In mature chicken NL neurons, AMPA-Rs lack the GluA2 subunit and show characteristic inward rectification when the membrane potential is depolarized. To test whether AMPA-Rs of GFP quail NL neurons also lack the GluA2 subunit, I–V relationships were recorded. The inset in Figure 10C shows isolated AMPA-R–mediated EPSCs from an E16 GFP quail NL neuron at various holding potentials, from which we constructed average I–V relationships (Fig. 10C). Both GFP quail and chicken neurons displayed a strong reduction in the outward flow of current mediated by isolated AMPA-Rs, consistent with inward rectification. The extent of rectification is summarized in Figure 10D by utilizing a rectification index ($RI = I_{AMPA\text{-}R}$ +40 mV/$I_{AMPA\text{-}R}$ −60 mV) as an indication of AMPA-Rs lacking the GluA2 subunit. The average rectification index was similar for GFP quail ($RI = 0.11 \pm 0.04$, $n = 12$) and chicken ($RI = 0.13 \pm 0.06$, $n = 7$). Taken together, the kinetics of GFP quail EPSCs along with the strong inward rectification suggest that AMPA-Rs lack the GluA2 subunit, a result consistent with previous reports in the chicken (Sanchez et al., 2010).

Synaptic depression of isolated AMPA-R–mediated EPSCs was seen when an E15 GFP quail NL neuron was voltage-clamped at −80 mV (to increase the driving force of Na^+) and afferent inputs were electrically stimulated at 100 Hz (Fig. 10E). Isolated AMPA-R–mediated EPSCs showed comparable synaptic depression in age-equivalent GFP quail and chicken NL neurons (Fig. 10F), suggesting that factors governing the depression of synaptic transmission are similar.

Synaptic AP properties of NL neurons

Mature auditory neurons have synaptic responses that are extremely brief in order to accommodate rapid, high-fidelity neural transmission. Electrical stimulation of afferent inputs from NM in GFP quail resulted in extremely brief, truncated, and highly reliable synaptic APs. Representative traces after low-frequency stimulation (0.1 Hz) are overlaid in Figure 10G from E14 GFP quail NL neurons. AP height and kinetics were highly consistent across all GFP quail NL neurons tested (Fig. 10H) and are in close agreement with synaptic properties reported for age-equivalent chicken NL neurons. These synaptic AP properties were highly sensitive to bath application of an AMPA-R antagonist (NBQX), a K_{LVA} blocker (DTX-I), or a K_{HVA} blocker (fluoxetine, data not shown), implying that AMPA-Rs and K^+ channels contribute to the highly specialized features found in time-coding neurons of the GFP quail auditory brainstem.

Afferent influences in NM and NL

Afferent inputs influence cell survival in NM and dendritic structure in NL in young chickens (Deitch and Rubel, 1984; Born and Rubel, 1985; Wang and Rubel, 2008). We analyzed NM cell number and dendrite structure of NL in posthatch GFP quail 6 days after unilateral cochlea removal. The NM ipsilateral to the silenced input exhibited a significant decrease in the volume of the nucleus and the number of neurons (Fig. 11A), compared with the contralateral NM, which continued to receive intact inputs (Fig. 11B).

Unilateral cochlea removal deprives excitatory inputs to the dorsal domain of the ipsilateral NL and the ventral

domain of the contralateral NL. Six days after cochlea removal, we found a dramatic decrease in the width of the afferent-deprived dendritic domain compared with the control domain of the same NL (Fig. 11C,D). Similar structural changes have been found in young chickens following deafferentation (Deitch and Rubel, 1984). In addition, dendritic reorganization of NL neurons may share common mechanisms in both avian species. Preceding dendritic retraction in deprived NL dendrites, we observed robust decreases in MAP2 immunoreactivity. This occurred as early as 3 hours and was still present at 1 day following the manipulation (Fig. 11E,F). This mirrors findings in the young chicken brain (Wang and Rubel, 2008).

DISCUSSION

During the last three decades, animal models in which genetic manipulations and high-resolution imaging are possible have become phenomenally important. In particular, mouse transgenic models have been powerful tools for studying the structure, function, and development of the mammalian brain. However, much of our knowledge about common principles of neural organization has

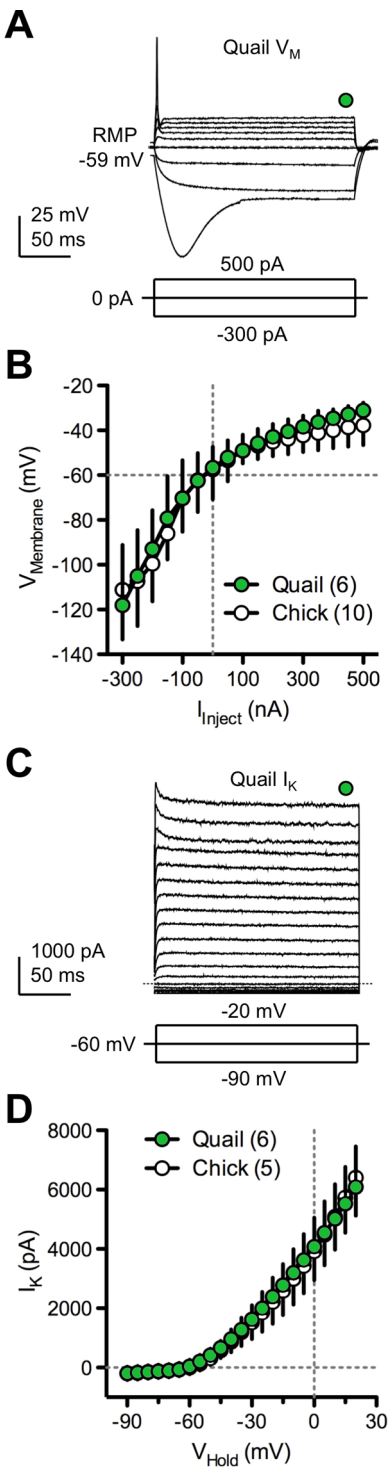

Figure 9. Specialized intrinsic properties of GFP quail NL neurons. **A:** Representative traces obtained in current-clamp configuration with bath application of AMPA-R, NMDA-R, and $GABA_A$-R antagonist (NBQX, 20 μM; DL-APV, 100 μM; and PTX, 100 μM, respectively). Example of superimposed membrane voltage responses (V_M) recorded while currents were injected into the soma of an E16 GFP quail NL neuron (top). Injected current range was −300 to 500 pA; duration, 200 ms; steps, 50 pA. Only three current steps are shown for clarity (bottom). Green circle above traces indicates time at which steady-state membrane potentials were measured (average of 5 ms between 180 and 185 ms of the membrane voltage) to obtain the voltage–current (V–I) relationships shown in B. All neurons tested ($n = 6$) responded to depolarizing steps with a single action potential. RMP, resting membrane potential. **B:** Average steady-state V–I relationships (GFP quail; white circles, $n = 6$, age E14–16). For comparison, age-equivalent chicken V–I relationships are superimposed (white circles, $n = 10$, age E19–21). Note: quail hatch in 16 days and chicks in 21 days. The flattened V–I function is indicative of low input resistance and large K^+ conductances. **C:** Representative traces obtained in voltage-clamp configuration with bath application of NBQX, DL-APV, PTX, and the Na^+ channel blocker TTX (0.1 μM). Example of superimposed potassium currents (I_K) recorded while voltage clamping an E15 GFP quail NL neuron at −60 mV (top). A range of voltage commands were applied from −90 to 20 pA; duration, 200 ms; steps, 5 pA. Only three voltage commands are shown for clarity (bottom). Green circle above traces indicates time at which steady-state current responses were measured (average of 5 ms between 180 and 185 ms of the membrane current) to obtain current–voltage (I–V) relationships shown in D. **D:** Average steady-state I–V relationships (GFP quail; white circles, $n = 6$, age E14–16). For comparison, age-equivalent chicken I–V relationships are superimposed (white circles, $n = 5$, age E19–21). Both GFP quail and chicken currents were sensitive to bath application of specific K^+ blockers, DTX-I (0.1 μM) and fluoxetine (100 μM) (data not shown). Currents were leak subtracted by using the recorded responses to hyperpolarizing voltage commands (−80 to −90 mV) as a baseline. Error bars in this and subsequent figures represent ±1 standard deviation. Stimulus artifacts are removed for clarity. [Color figure can be viewed in the online issue, which is available at wileyonlinelibrary.com.]

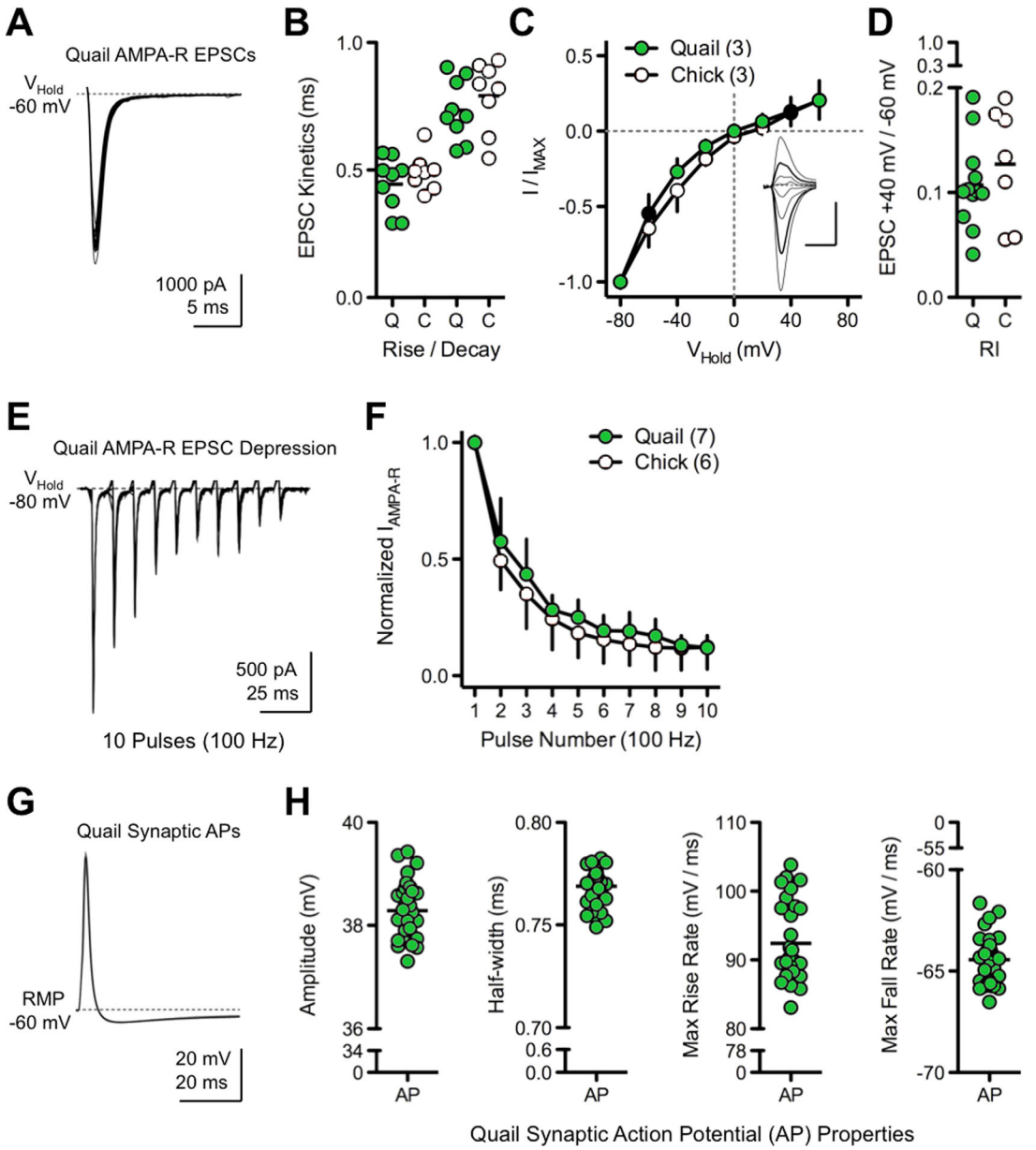

Figure 10. Specialized synaptic properties of GFP quail NL neurons. **A:** Representative traces obtained in voltage-clamp configuration with bath application of DL-APV and PTX. Patch pipettes contained a CsCl/QX-314 internal solution to block K^+ and Na^+ channel conductances, respectively. Example of superimposed isolated AMPA-R–mediated excitatory postsynaptic currents (EPSCs) recorded from an E14 GFP quail NL neuron while voltage clamping the neuron at −60 mV and electrically stimulating afferent inputs from the ipsilateral nucleus magnocellularis (NM). **B:** Population data showing isolated AMPA-R–mediated EPSC kinetics (rise and decay tau, fit with a single exponential) for GFP quail (Q; green circles, $n = 9$, age E14–16) and chicken (C; white circles, $n = 8$, age E19). **C:** Normalized isolated AMPA-R–mediated I-V relationships for GFP quail (green circles, $n = 3$, age E14–16) and chicken (white circles, $n = 3$, age E19). Inset shows representative superimposed isolated AMPA-R–mediated EPSCs recorded at different holding voltages (−80 mV to +60 mV, steps 20 mV) from an E16 GFP quail NL neuron. Vertical scale bar: 500 pA, horizontal scale bar: 2 ms. Thick black traces in inset and black circles in population graph represent currents recorded at +40 mV and −60 mV to derive rectification indexes shown in D. I-V recording were obtained with spermine (100 μM) added to pipette internal solution to block the ion channel of GluA2-lacking AMPA-Rs in a voltage-dependent manner. **D:** Population data showing rectification index ($I_{AMP\text{-}R}$ +40 mV/$I_{AMPA\text{-}R}$ −60 mV; see Materials and Methods) for GFP quail (Q; green circles, $n = 12$, age E14–16) and chicken (C; white circles, $n = 7$, age E19). Rapid kinetics and strong inward rectification are indicative of AMPA-Rs lacking the GluA2 receptor subunit. **E:** Example of superimposed isolated AMPA-R–mediated EPSCs ($n = 11$) recorded from an E15 GFP quail NL neuron while voltage clamping the neuron at −80 mV and electrically stimulating afferent inputs at a rate of 100 Hz. **F:** Normalized population data from GFP quail (green circles, $n = 7$, age E14–16) and chicken (white circles, $n = 6$, age E19–21) showing strong isolated AMPA-R–mediated EPSC depression. **G:** Representative traces obtained in current-clamp configuration with bath application of PTX. Example of superimposed synaptic action potentials (APs) recorded from an E14 GFP quail NL neuron while electrically stimulating afferent inputs from the ipsilateral NM. **H:** Population data of GFP quail synaptic AP properties (age E14–16, $n = 4$, 10–11 APs each). [Color figure can be viewed in the online issue, which is available at wileyonlinelibrary.com.]

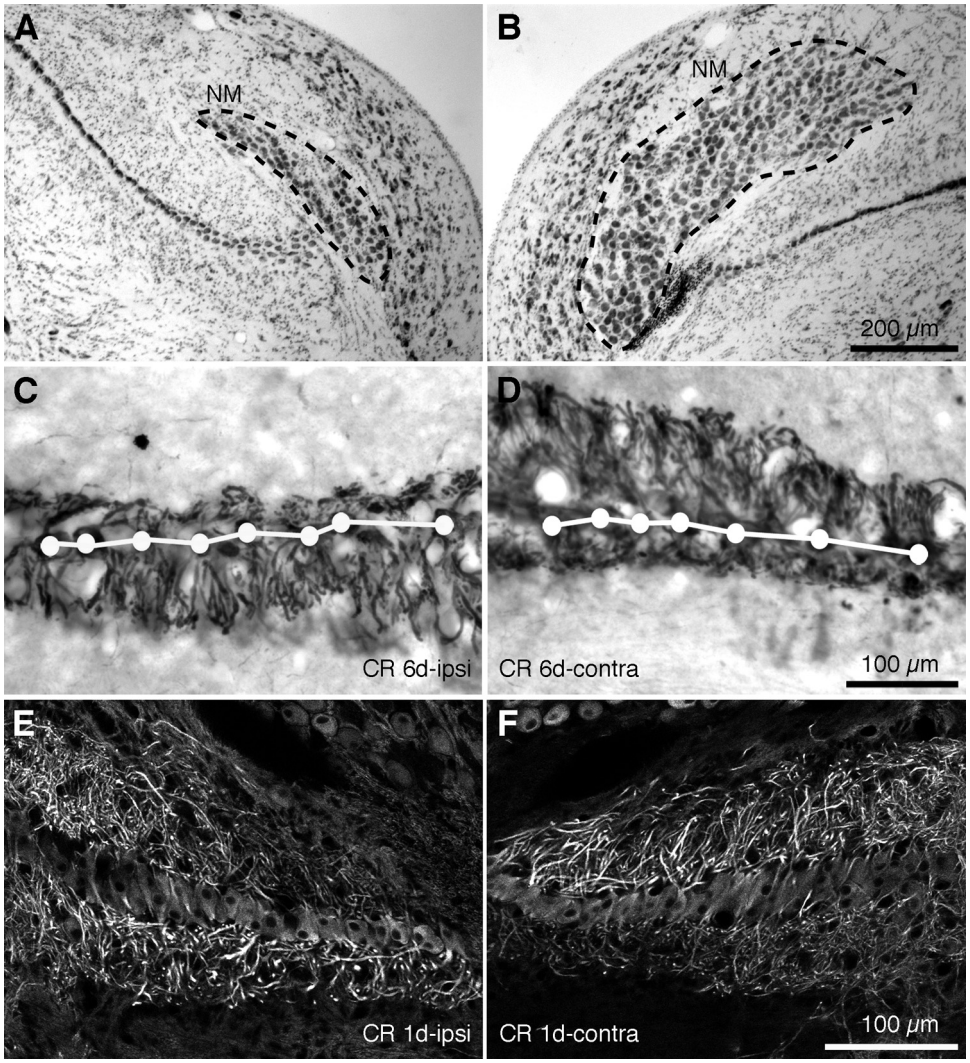

Figure 11. Afferent influence on cell survival of NM neurons and NL dendritic structure in transgenic quail. **A,B:** Following unilateral cochlea removal, there are decreases in the cell number and the size of the nucleus in the ipsilateral NM (A), compared with the intact contralateral NM (B). Images were taken from an animal that survived for 6 days following the surgery. Dashed lines outline the boundary of NM. **C,D:** At 6 days following cochlea removal, dramatic dendritic retraction was detected in the dorsal dendritic domain of the ipsilateral NL (C) and the ventral domain of the contralateral NL (D). **E,F:** At 1 day following cochlea removal, deprived dendritic domains in NL exhibited notable decreases in MAP2 immunoreactivity. White dots and lines in C and D indicate the location of the somata. Scale bar = 200 μm in B (applies to A,B); 100 μm in D (applies to C,D) and F (applies to E,F).

come from studies of diverse vertebrate and invertebrate organisms. Studies of the mature avian brain, for example, have provided important clues about fundamental principles of forebrain evolution (e.g., Wang et al., 2010). More relevant to the current work, experimental studies of embryonic chickens have added much to our understanding of vertebrate embryonic nervous system development. Until recently, the availability of genetic techniques, such as the production of transgenic and knockout animal models, has been limited in the avian system. However, the Japanese quail has proved to be an excellent model organism for the production of transgenic avians using lentiviral vectors (Scott and Lois, 2005; Poynter et al., 2009). Current HIV-based lentiviral vectors are able to package relatively large constructs (up to 8 kb), which allows for the use of many cell-specific promoters and various reporter molecules. Once the transgene is integrated into the genome of the host animal, it does not appear to be highly subject to silencing, as is the case with other classes of retroviruses. The high degree of homology between chicken and quail genomes (Hillier, 2004; Wallis et al., 2004) allows researchers to design avian-specific DNA constructs for the production of transgenic quail. Highly conserved regions of mammalian genes can also be used to produce transgenic quail, as the current study shows.

Sequencing of the quail genome will allow for increasing numbers of quail-specific constructs to be generated in the future. The relatively small size of the adults, short time to sexual maturity, and abundant egg production of the Japanese quail make the development of transgenic lines less labor- and space-intensive compared with chickens. In addition, transgenic quail offer all the advantages of the classic avian developmental model system, such as the ability to culture the embryos in vitro and utilize quail/chicken transplant chimeras (Teillet et al., 2008). Finally, dynamic time-lapse confocal imaging of transgenic Japanese quail embryos expressing fluorescent reporters is ideal for examining complex cell and tissue movements during development (Sato et al., 2010).

Our main goal was to determine the degree of similarity between a well-studied avian model system, the chicken auditory brainstem, and that of the novel transgenic GFP quail (Scott and Lois, 2005). The hearing range and sensitivity of quail and chicken are very similar (Niemiec et al., 1994), facilitating direct comparisons of auditory structure and function between the species. By utilizing the well-established circuitry of the chicken auditory brainstem for direct comparison, we found the GFP quail to be a suitable alternative model organism to study the avian nervous system. We conclude that in GFP quail, the structure and function of the auditory brainstem is indistinguishable from its equivalent in the chicken. The production of the transgenic quail and the comparison between specific form and function are discussed in greater detail below.

Similarities between the GFP quail and the chicken auditory brainstem

A large number of unique structural and functional features of the brainstem auditory pathways have been described over the past 40 years. These specialized features are thought to be essential for the computation of interaural time differences (ITDs), a computation required for sound localization and auditory segmentation (for review, see Burger and Rubel, 2008). Structural features of NM and NL in the GFP quail were virtually indistinguishable from those of the chicken with respect to general cytoarchitecture, innervation patterns (excitatory and inhibitory), detailed morphology of axonal terminal endings, subcellular distribution of receptors and ion channels, and physiological properties. Based on these similarities, it was not surprising that neuronal cell number and dendritic structure of these neurons from the GFP quail are dynamically regulated by excitatory afferent inputs in similar ways to those observed in the chicken (Born and Rubel, 1985; Wang and Rubel, 2008).

Potassium channel distribution in NM and NL of the GFP quail

Quail NL neurons, like those of the chicken (Lu et al., 2004; Kuba et al., 2005), strongly express low-voltage activated potassium channels (K_{LVA}). Interestingly, in the GFP quail, the expression of the Kv1.2 staining in NL at E14, an embryonic age equivalent to E19 in chicken, is highest on the proximal axon, a pattern recently described in age-matched chicken NL neurons (Sanchez et al., in press). Similar expression patterns have been observed in auditory nuclei involved in the processing of temporally precise information (Dodson et al., 2002) and other neurons in the mammalian cerebral cortex, retinal ganglion cells, and elsewhere (Inda et al., 2006; Van Wart et al., 2007; Shu et al., 2007; Kole et al., 2007; Lorincz and Nusser, 2008). We speculate that this expression pattern is required for the characteristic spiking pattern exhibited by NL neurons.

General function of NL neurons in the GFP quail

We found a striking resemblance between the physiological properties of age-matched chickens and GFP quail, including: 1) similar intrinsic membrane responses to somatic current injections; 2) strong K^+ channel conductances; 3) fast kinetics and strong synaptic depression of AMPA-R–mediated EPSCs; and 4) reliable and rapid synaptic AP generation. Thus, age-equivalent GFP quail NL neurons appear to contain several highly specialized membrane properties found in chicken embryos.

It needs to be determined, however, whether NL neurons in the GFP quail show the same response characteristics in vivo as they do in chicken. Of particular interest would be their ITD tuning properties, as shown for NL neurons in barn owl (Carr and Konishi, 1990) and chicken (Köppl and Carr, 2008). However, we see the main advantage of the GFP quail animal model for in vitro applications, for which imaging of neurons can be combined with manipulations and/or electrophysiological recordings.

Transgenic quail as an avian model organism

For decades, the avian peripheral and central nervous system has been used to study numerous basic biological processes and was the dominant animal for studies of nervous system development for most of the 20th century. With the advent of powerful genetic tools in invertebrates and mice, there has been a dramatic decrease in the use of avian embryos and thus the large body of information that past research has provided. Now, transgenic quail, including the neuronal-specific eGFP lines

described here, constitute a powerful new addition that may prove useful for future studies of comparative and developmental neurobiology.

ACKNOWLEDGMENT

We thank Dale Cunningham for assistance with the embryonic tissue preparation and sectioning, Glen MacDonald for help with microscopy, and Andrés Barría for use of equipment. We also thank Mark Bothwell, Melissa Strong, and the anonymous reviewers for comments on the manuscript.

CONFLICT OF INTEREST STATEMENT

The authors state there is no conflict of interest.

ROLE OF AUTHORS

All authors had full access to all the data in the study and take responsibility for the integrity of the data and the accuracy of the data analysis. Study concept and design: A.H.S., J.T.S., L.S., K.M.T., Y.W., D.T.K., E.W.R., R.L. Acquisition of data: A.H.S., J.T.S., L.S., K.M.T., Y.W., D.T.K., G.P., D.H. Analysis and interpretation of data: A.H.S., J.T.S., L.S., K.M.T., Y.W., D.T.K., G.P., D.H., R.L., E.W.R. Drafting of the manuscript: A.H.S., J.T.S., L.S., K.M.T., Y.W., E.W.R. Comments on the manuscript: D.H., R.L. Production of transgenic quail: G.P., D.H., S.E.F., R.L. Obtained funding: E.W.R., R.L., S.E.F.

LITERATURE CITED

Born DE, Rubel EW. 1985. Afferent influences on brain stem auditory nuclei of the chicken: neuron number and size following cochlea removal. J Comp Neurol 231:435–445.

Bosselman RA, Hsu RY, Boggs T, Hu S, Bruszewski J, Ou S, Kozar L, Martin F, Green C, Jacobsen F. 1989. Germline transmission of exogenous genes in the chicken. Science 243:533–535.

Burger RM, Rubel EW. 2008. Encoding of interaural timing for binaural hearing. In: Basbaum AI, Kaneko A, Sheperd GM, Westheimer G, eds. The Senses: A Comprehensive Reference. Vol 3, Audition, Dallos P, Oertel D, eds. San Diego: Academic Press. p 613–630.

Burger RM, Cramer KS, Pfeiffer JD, Rubel EW. 2005. Avian superior olivary nucleus provides divergent inhibitory input to parallel auditory pathways. J Comp Neurol 481:6–18.

Burger RM, Fukui I, Ohmori H, Rubel EW. 2011. Inhibition in the balance: binaurally coupled inhibitory feedback in sound localization circuitry. J Neurophysiol 106:4–14.

Carr CE, Konishi M. 1990. A circuit for detection of interaural time differences in the brain stem of the barn owl. J Neurosci 10:3227–3246.

Code RA, Churchill L. 1991. $GABA_A$ receptors in auditory brainstem nuclei of the chick during development and after cochlea removal. Hear Res 54:281–295.

Code RA, Burd GD, Rubel EW. 1989. Development of GABA immunoreactivity in brainstem auditory nuclei of the chick: ontogeny of gradients in terminal staining. J Comp Neurol 284:504–518.

Deitch JS, Rubel EW. 1984. Afferent influences on brain stem auditory nuclei of the chicken: time course and specificity of dendritic atrophy following deafferentation. J Comp Neurol 229:66–79.

Dittgen T, Nimmerjahn A, Komai S, Licznerski P, Waters J, Margrie TW, Helmchen F, Denk W, Brecht M, Osten P. 2004. Lentivirus-based genetic manipulations of cortical neurons and their optical and electrophysiological monitoring in vivo. Proc Natl Acad Sci U S A 101:18206–18211.

Dodson PD, Barker MC, Forsythe ID. 2002. Two heteromeric Kv1 potassium channels differentially regulate action potential firing. J Neurosci 22:6953–6961.

Dunn DA, Pinkert CA, Kooyman DL. 2005. Foundation Review: Transgenic animals and their impact on the drug discovery industry. Drug Discov Today 10:757–767.

Eyal-Giladi H, Kochav S. 1975. From cleavage to primitive streak formation; a complementary normal table and a new look at the first stages of the development of the chick. I. General morphology. Dev Biol 49:321–327.

Feng G, Mellor RH, Bernstein M, Keller-Peck C, Nguyen QT, Wallace M, Nerbonne JM, Lichtman JW, Sanes JR. 2000. Imaging neuronal subsets in transgenic mice expressing multiple spectral variants of GFP. Neuron 28:41–51.

Fritzsch B, Beisel KW, Jones K, Fariñas I, Maklad A, Lee J, Reichardt LF. 2002. Development and evolution of inner ear sensory epithelia and their innervation. J Neurobiol 53: 143–156.

Grutzendler J, Kasthuri N, Gan W-B. 2002. Long-term dendritic spine stability in the adult cortex. Nature 420:812–816.

Hillier LW. 2004. Sequence and comparative analysis of the chicken genome provide unique perspectives on vertebrate evolution. Nature 432:695–716.

Huss D, Poynter G, Lansford R. 2008. Japanese quail (*Coturnix japonica*) as a laboratory animal model. Lab Anim (NY) 37: 513–519.

Hyson RL. 2005. The analysis of interaural time differences in the chick brain stem. Physiol Behav 86:297–305.

Inda MC, DeFelipe J, Muñoz A. 2006. Voltage-gated ion channels in the axon initial segment of human cortical pyramidal cells and their relationship with chandelier cells. Proc Natl Acad Sci U S A 103:2920–2925.

Jaenisch R. 1988. Transgenic animals. Science 240:1468–1474.

Jhaveri S, Morest DK. 1982. Neuronal architecture in nucleus magnocellularis of the chicken auditory system with observations on nucleus laminaris: a light and electron microscope study. Neuroscience 7:809–836.

Kole MHP, Letzkus JJ, Stuart GJ. 2007. Axon initial segment Kv1 channels control axonal action potential waveform and synaptic efficacy. Neuron 55:633–647.

Köppl C, Carr CE. 2008. Maps of interaural time difference in the chicken's brainstem nucleus laminaris. Biol Cybern 98: 541–559.

Kuba H, Yamada R, Fukui I, Ohmori H. 2005. Tonotopic specialization of auditory coincidence detection in nucleus laminaris of the chick. J Neurosci 25:1924–1934.

Kubke MF, Carr CE. 2000. Development of the auditory brainstem of birds: comparison between barn owls and chickens. Hear Res 147:1–20.

Kuo SP, Bradley LA, Trussell LO. 2009. Heterogeneous kinetics and pharmacology of synaptic inhibition in the chick auditory brainstem. J Neurosci 29:9625–9634.

Lendvai B, Stern EA, Chen B, Svoboda K. 2000. Experience-dependent plasticity of dendritic spines in the developing rat barrel cortex in vivo. Nature 404:876–881.

Lorincz A, Nusser Z. 2008. Cell-type-dependent molecular composition of the axon initial segment. J Neurosci 28: 14329–14340.

Lu Y, Monsivais P, Tempel BL, Rubel EW. 2004. Activity-dependent regulation of the potassium channel subunits Kv1.1 and Kv3.1. J Comp Neurol 470:93–106.

Matus A, Bernhardt R, Hugh-Jones T. 1981. High molecular weight microtubule-associated proteins are preferentially associated with dendritic microtubules in brain. Proc Natl Acad Sci U S A 78:3010–3014.

Mozdziak PE, Borwornpinyo S, McCoy DW, Petitte JN. 2003. Development of transgenic chickens expressing bacterial beta-galactosidase. Dev Dyn 226:439–445.

Nägerl UV, Köstinger G, Anderson JC, Martin KAC, Bonhoeffer T. 2007. Protracted synaptogenesis after activity-dependent spinogenesis in hippocampal neurons. J Neurosci 27: 8149–8156.

Niemiec AJ, Raphael Y, Moody DB. 1994. Return of auditory function following structural regeneration after acoustic trauma: behavioral measures from quail. Hear Res 79: 1–16.

Nishino E, Yamada R, Kuba H, Hioki H, Furuta T, Kaneko T, Ohmori H. 2008. Sound-intensity-dependent compensation for the small interaural time difference cue for sound source localization. J Neurosci 28:7153–7164.

Parks TN, Rubel EW. 1978. Organization and development of the brain stem auditory nuclei of the chicken: primary afferent projections. J Comp Neurol 180:439–448.

Perry MM, Sang HM. 1993. Transgenesis in chickens. Transgenic Res 2:125–133.

Pfeiffer F, Simler R, Grenningloh G, Betz H. 1984. Monoclonal antibodies and peptide mapping reveal structural similarities between the subunits of the glycine receptor of rat spinal cord. Proc Natl Acad Sci U S A 81: 7224–7227.

Portera-Cailliau C, Weimer RM, De Paola V, Caroni P, Svoboda K. 2005. Diverse modes of axon elaboration in the developing neocortex. PLoS Biol 3:e272–e272.

Poynter G, Huss D, Lansford R. 2009. Japanese quail: an efficient animal model for the production of transgenic avians. Cold Spring Harb Protoc 2009:pdb.emo112.

Rubel EW, Smith DJ, Miller LC. 1976. Organization and development of brain stem auditory nuclei of the chicken: ontogeny of n. magnocellularis and n. laminaris. J Comp Neurol 166:469–489.

Rubel EW, Hyson RL, Durham D. 1990. Afferent regulation of neurons in the brain stem auditory system. J Neurobiol 21: 169–196.

Salter DW, Smith EJ, Hughes SH, Wright SE, Crittenden LB. 1987. Transgenic chickens: insertion of retroviral genes into the chicken germ line. Virology 157:236–240.

Sambrook J, Russell DW. 2001. Molecular cloning: a laboratory manual. Cold Spring Harbor, NY: Cold Spring Harbor Laboratory Press.

Sanchez JT, Wang Y, Rubel EW, Barria A. 2010. Development of glutamatergic synaptic transmission in binaural auditory neurons. J Neurophysiol 104:1774–1789.

Sang H. 2004. Prospects for transgenesis in the chick. Mech Dev 121:1179–1186.

Sato Y, Poynter G, Huss D, Filla MB, Czirok A, Rongish BJ, Little CD, Fraser SE, Lansford R. 2010. Dynamic analysis of vascular morphogenesis using transgenic quail embryos. PLoS One 5:e12674.

Scott BB, Lois C. 2005. Generation of tissue-specific transgenic birds with lentiviral vectors. Proc Natl Acad Sci U S A 102:16443–16447.

Seidl AH, Rubel EW, Harris DM. 2010. Mechanisms for adjusting interaural time differences to achieve binaural coincidence detection. J Neurosci 30:70–80.

Shu Y, Yu Y, Yang J, McCormick DA. 2007. Selective control of cortical axonal spikes by a slowly inactivating K^+ current. Proc Natl Acad Sci U S A 104:11453–11458.

Smith DJ, Rubel EW. 1979. Organization and development of brain stem auditory nuclei of the chicken: dendritic gradients in nucleus laminaris. J Comp Neurol 186:213–239.

Smith ZD. 1981. Organization and development of brain stem auditory nuclei of the chicken: dendritic development in N. laminaris. J Comp Neurol 203:309–333.

Tabor KM, Wong RO, Rubel EW. 2011. Topography and morphology of the inhibitory projection from superior olivary nucleus to nucleus laminaris in chickens (*Gallus gallus*). J Comp Neurol 519:358–375.

Teillet M-A, Ziller C, Le Douarin NM. 2008. Quail-chick chimeras. Methods Mol Biol 461:337–350.

Trachtenberg JT, Chen BE, Knott GW, Feng G, Sanes JR, Welker E, Svoboda K. 2002. Long-term in vivo imaging of experience-dependent synaptic plasticity in adult cortex. Nature 420:788–794.

Van Wart A, Trimmer JS, Matthews G. 2007. Polarized distribution of ion channels within microdomains of the axon initial segment. J Comp Neurol 500:339–352.

Wallis JW, Aerts J, Groenen MAM, Crooijmans RPMA, Layman D, Graves TA, Scheer DE, Kremitzki C, Fedele MJ, Mudd NK, Cardenas M, Higginbotham J, Carter J, McGrane R, Gaige T, Mead K, Walker J, Albracht D, Davito J, Yang S-P, Leong S, Chinwalla A, Sekhon M, Wylie K, Dodgson J, Romanov MN, Cheng H, de Jong PJ, Osoegawa K, Nefedov M, Zhang H, McPherson JD, Krzywinski M, Schein J, Hillier L, Mardis ER, Wilson RK, Warren WC. 2004. A physical map of the chicken genome. Nature 432:761–764.

Wang Y, Rubel EW. 2008. Rapid regulation of microtubule-associated protein 2 in dendrites of nucleus laminaris of the chick following deprivation of afferent activity. Neuroscience 154:381–389.

Wang Y, Cunningham DE, Tempel BL, Rubel EW. 2009. Compartment-specific regulation of plasma membrane calcium ATPase type 2 in the chick auditory brainstem. J Comp Neurol 514:624–640.

Wang Y, Brzozowska-Prechtl A, Karten HJ. 2010. Laminar and columnar auditory cortex in avian brain. Proc Natl Acad Sci U S A 107:12676–12681.

Young SR, Rubel EW. 1983. Frequency-specific projections of individual neurons in chick brainstem auditory nuclei. J Neurosci 3:1373–1378.

Zajchowski LD, Etches RJ. 2000. Transgenic chickens: past, present, and future. Avian Poultry Biol Rev 11:63–80.